

# COMPARING THE GAMBINI'S ALGORITHM AND A CFAR METHOD TO EDGE DETECTION FOR POLSAR IMAGES

*Anderson A. de Borba<sup>a</sup>, Maurício Marengoni<sup>b</sup>, and Alejandro C. Frery<sup>c</sup>.*

<sup>a</sup>IBMEC-SP, Alameda Santos, 2356 - Jardim Paulista, SP – Brazil,

<sup>b</sup>Albion College, Albion, MI – USA,

<sup>c</sup>School of Mathematics and Statistics, Victoria University of Wellington, 6140, New Zealand.

## ABSTRACT

In this work we compare two different method to detect edges for PolSAR images. The Gambini's algorithm and a simple CFAR method (The Coefficient of Variation Detector). Both methods were able to detect edges in the simulated images used in this work. The Gambini's algorithm has the advantage of finding a single pixel as an edge while the CFAR method detects multiple edges, mainly when the edge is a ramp edge. In the other hand, the CFAR method can be directly applied to the images while the Gambini's algorithm needs to have as input a region of interest and lines where the transition point between distributions (edges) are detected.

**Index Terms**— Gambini's Algorithm, CFAR coefficient of variation, edge detection.

## 1. INTRODUCTION

The present research aims to compare two different methods to find edges in PolSAR images. The first method is the Gambini's algorithm (GA) (see Refs. [1, 2]) which is not an edge detector but a method to find the transition point between two Gamma distributions, as different areas in the ground will respond differently for a PolSAR signal the transition point between these two areas can be seen as an edge. The second method is a Constant False Alarm Rate (CFAR) - Coefficient of Variation Detector (see Ref. [3]) where a coefficient of variation is used to find edges in PolSAR images. Simulated images were used in this research, a simple rectangle area in the middle of the image. Nine different images were used, three with a sharp edge and six with a ramp edge.

In Refs [1, 2], Gambini et al. used the  $\mathcal{G}^0$  polarimetric distributions (see Refs [4, 5]). In Refs. [6, 7], Borba et al. modified the polarimetric  $\mathcal{G}^0$  distribution to the Wishart distribution applying it to PolSAR images. The simulated images were drawn from the works of [8, 9].

Refs. [3] and [10] presents some CFAR-type methods. This work presented here implements the idea proposed in [3] for the CFAR method coefficient of variation detector.

e-mail:<sup>a</sup>anderson.aborba@professores.ibmec.edu.br,  
<sup>b</sup>mmarengoni@albion.edu, <sup>c</sup>alejandro.frery@vuw.ac.nz

It is essential to highlight the difference between the Gambini algorithm and the CFAR methods. It is known that PolSAR images have multiplicative noise known as speckle. GA uses the Speckle noise as an ally; that is, no treatment such as filtering is performed. On the other hand, in CFAR-like methods, the speckle noise is treated with filtering processes.

The article is structured as follows. Section 2 describes the simulated image tests. Section 3 highlight the Gambini Algorithm (GA) to edge detection and describe CFAR coefficient of variation detect methods . Section 4 presents the results. Finally, in Section 5 we discuss the results.

## 2. SIMULATED IMAGES

Based on Refs [8,9], we get the simulated images with dimension  $800 \times 800 \times 3$  with two classes, the third dimension is a channel number. To achieve this goal, we built a reference image as follows:

- Set 0 to all pixels in the image.
- Insert a rectangle  $[x_l, x_u] \times [y_l, y_u]$  centered at the pixel  $(x_c, y_c) = (400, 400)$ , for all channels, where  $x_l = x_c - 100$ , is the lower horizontal coordinate,  $x_u = x_c + 100$ , is the upper horizontal coordinate,  $y_l = y_c - 50$ , is the lower vertical coordinate,  $y_u = y_c + 50$ , is the upper vertical coordinate, and  $\epsilon$ , is the ramp constant.
- Set 1 for pixels inside the rectangle and its boundary,

We define the function (1) in the horizontal ramps  $[x_l + \epsilon, x_u - \epsilon] \times [y_l - \epsilon, y_l + \epsilon]$ , and  $[x_l + \epsilon, x_u - \epsilon] \times [y_u - \epsilon, y_u + \epsilon]$ . And, the same way in the vertical ramps  $[x_l - \epsilon, x_l + \epsilon] \times [y_l + \epsilon, y_u - \epsilon]$ , and  $[x_u - \epsilon, x_u + \epsilon] \times [y_l + \epsilon, y_u - \epsilon]$ .

We use function (2), on the corners.

The outer region in the simulated image is the complementary region of the ramp, defined around the rectangle, plus the internal region of the rectangle.

The function for the horizontal ramps is:

$$f_x(x) = \begin{cases} 0 & \text{if } x < 0 \\ 6x^5 - 15x^4 + 10x^3 & \text{if } 0 \leq x \leq 1 \\ 1 & \text{if } x > 1. \end{cases} \quad (1)$$

The function for the corners is:

$$f(x, y) = f_x(x) \cdot f_y(y), \quad \text{with } (x, y) \in \mathbb{R}^2 \quad (2)$$

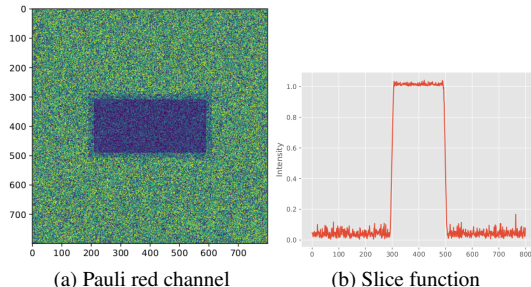
The reference image is defined as  $R_1$ . In addition to this image, we define two more images,  $R_2$ , which we call the negative image of  $R_1$ . It consists of switching the values of 0 and 1 in the image. Similarly, in  $R_3$ , we switched the values of 0 by 5 and the values of 1 by 10. In both cases, the functions from 1 to 2 are modified accordingly.

Three images tests based on the procedure above were defined. First, the image test  $T_1$ , based on  $R_1$ , was defined using Wishart distribution with  $\mu_1$  added in the outer region,  $\mu_2$  added in the internal rectangle and  $\mu_{av} = (\mu_1 + \mu_2)/2$  added in the ramps. The parameter  $L = 4$  is the same for all regions.

Second, the image test  $T_2$  and  $T_3$  were built similarly to image test  $T_1$ .

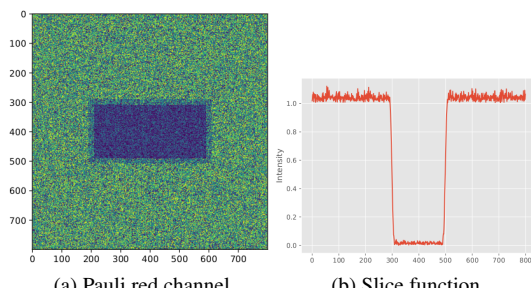
The parameters used for the Wishart distribution in the HH channel are HH are  $\mu_1 = 0.042811$ , and  $\mu_2 = 0.014380$ :

Fig. 1 shows the red channel of the Pauli decomposition of image  $T_1$  and the slice of the function at coordinate 400 showing the ramp between the two areas.



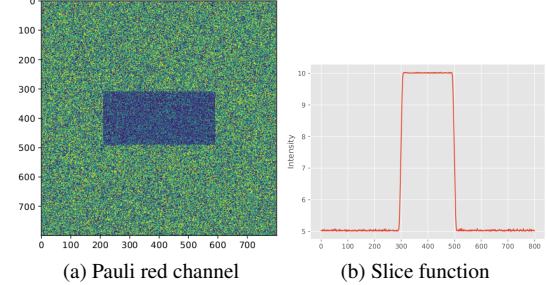
**Fig. 1.** Image  $T_1$  and the slice function for  $\epsilon = 10$

Fig. 2 shows the red channel of the Pauli decomposition of image  $T_2$  and the slice of the function is similar with Fig. 1



**Fig. 2.** Image  $T_2$  and its slice function with  $\epsilon = 10$

Fig. 3 shows the red channel of the Pauli decomposition of image  $T_3$  and the slice of the function is similar with Fig. 1



**Fig. 3.** Image  $T_3$  and its slice function with  $\epsilon = 10$

### 3. EDGE DETECTION

In this work, we compare two popular methods to find edges in PolSAR images, the GA and a Constant False Alarm Rate (CFAR) that uses the coefficient of variation detector.

#### 3.1. Gambini's algorithm – GA

The GA is actually not an edge detector. It's main purpose is to find the transition point between two different Gamma distributions in neighbor areas. This transition point can be seen, and have been used as an edge detector. The algorithm is presented in Refs. [1, 2], and they are based on the density distributions  $\mathcal{G}^0$ , that can be found in Refs. [4, 5]. We modified the algorithm to apply in Wishart distributions from PolSAR images. The method is described in Refs. [6, 7].

#### 3.2. CFAR Coefficient of Variation Detector

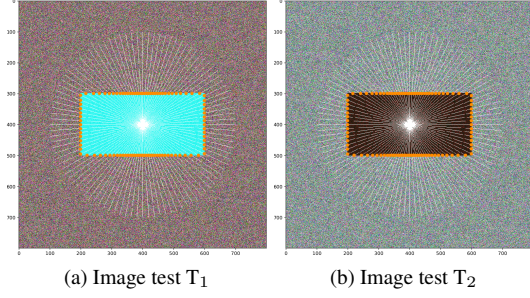
One of the methods shown in Refs [9] is called CFAR Coefficient of Variation Detector. It is a CFAR type method known for edge detection in radar images implemented as follows:

- Calculate the mean  $M$  for the center pixel defined by the sliding window with dimension  $N = n \times n$  pixels, where  $n$  is the width and height of the window.  $M = (\sum_{i=1}^N x_i)/N$ .
- Calculate the standard deviation  $S$  for the center pixel using the same window before.  $S = \sqrt{\sum_{i=1}^N (x_i - M)^2}/N - 1$ .
- For each pixel, calculate the ratio  $r = S/M$ .
- Compare  $r$  to the threshold  $\ell_1 = 1/\sqrt{L} + \tau$ , where  $L$  is the multi-look parameter. Large values of  $r$  are considered edge evidence, then if  $r > \ell_1$ , set the pixel as an edge.

### 4. RESULTS

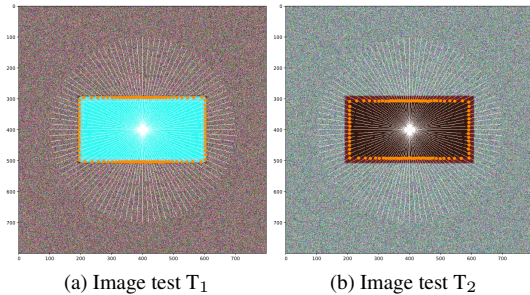
We applied the GA in test images  $T_1$ ,  $T_2$ , and  $T_3$ . Tests were performed for  $\epsilon$  equals 0 and 10. The results were different for these two cases.

Fig. 4 shows edges evidences detected for image test T<sub>1</sub> and T<sub>2</sub>. We can see that GA presents similar results for both images and no outliers.



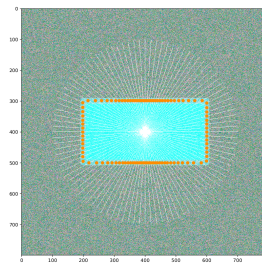
**Fig. 4.** Edge evidences to images test T<sub>1</sub> and T<sub>2</sub> with  $\epsilon = 0$

Fig. 5 shows edges evidences detected when we added a ramp around the internal rectangle. Fig. 5(a) shows edge evidence near the outer region. Fig 5(b) shows edge evidence internal to the rectangle. Therefore, we can note that edges evidences are detected when the sample value goes to zero in the image test T<sub>1</sub> and T<sub>2</sub>.



**Fig. 5.** Edge evidences to images test T<sub>1</sub> and T<sub>2</sub> with  $\epsilon = 10$

Looking at the results presented in Fig. 5 we thought that the area with the 0 value could be a problem, so we decided to create image tests T<sub>3</sub> and T<sub>4</sub> (not shown here) with  $\epsilon = 10$  and applied the GA to these images. In both cases the result was the same as presented in Fig. 6 with the edge at about the center of the ramp.



**Fig. 6.** Edge evidences to image test T<sub>3</sub> with  $\epsilon = 10$

The Coefficient of Variation Detector was applied to image test T<sub>1</sub> and T<sub>2</sub>, and the results are shown in Figs. 7. We configured the method with a kernel value equals to  $3 \times 3$ , and  $\tau = 0.3$ , to control the threshold value and reduce outliers.

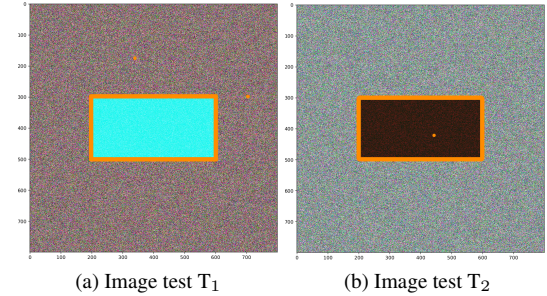


**Fig. 7.** Edge evidences to images test T<sub>1</sub> and T<sub>2</sub> with  $\epsilon = 0$

Because of the outliers shown in Fig 7. we changed the CFAR parameters using a  $5 \times 5$  kernel and  $\tau$  equals 0.5. The result is presented in Fig. 8. In Figs. 8(a) and 8(b), we observe a similar behavior to GA. Evidence of edges was detected near the zero-based sample.

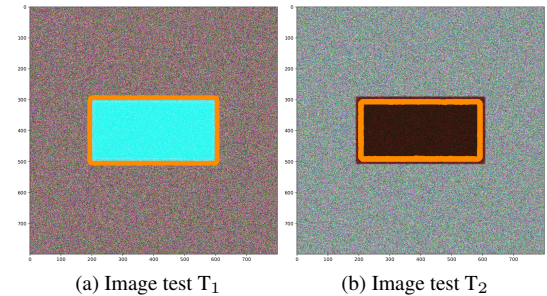


**Fig. 8.** Edge evidences to images test T<sub>1</sub> and T<sub>2</sub> with  $\epsilon = 10$

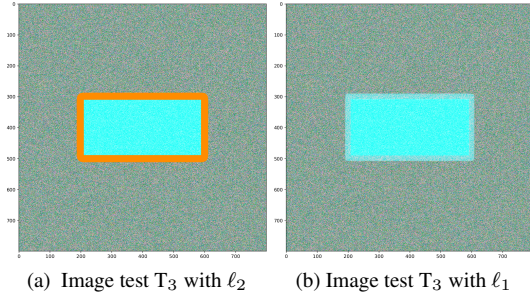
The Coefficient of Variation Detector was applied to image test T<sub>3</sub>, and the results are shown in Figs. 9. We configured the method with a kernel value equals to  $5 \times 5$ , and defined  $\ell_2$  as  $\frac{1}{5}\sqrt{L} + \tau$ . This threshold was defined empirically. The threshold original defined in Ref. [3] ( $\ell_1$ ) did not work well to test image T<sub>3</sub>. Fig. 9(b) shows that no edge evidence was detected with the  $\ell_1$  threshold.

Fig. 9(a) shows the edge evidence using the threshold  $\ell_2$  for the Coefficient of Variation Detector.

We emphasize that the tests performed to detect evidence of edges do not depend on the order between  $\mu_1$  and  $\mu_2$ . Also, all PolSAR channels show similar results to the HH channel used to generate the pictures presented in this paper.

We can highlight the following results:

- (i) When the tests are performed using T<sub>1</sub> and T<sub>2</sub>, the edge was detected near sample based on 0 for both detectors. The Coefficient of Variation Detector detects multiple



**Fig. 9.** Edge evidences to images test  $T_3$  with  $\epsilon = 10$

edges when there is a ramp edge in the image and needs further processing to refine its result. In this case the GA finds a single edge.

- (ii) When the tests were performed in  $T_3$  and its negative, the GA method finds edge evidence within the ramp.
- (iii) The Coefficient of Variation Detector is applied in  $T_1$ ,  $T_2$  and  $T_3$ , and there are arising outliers. We can note that the method has sensitivity in the choice of the  $\tau$  parameter.
- (iv) The Coefficient of Variation Detector is applied in  $T_3$ . In this case, the threshold does not respect the rule proposed in the article [3]. We propose empirically the threshold  $\ell_2 = \frac{1}{5}\sqrt{L} + \tau$  which showed good results visually.
- (v) In the Coefficient of Variation Detector with test image  $T_3$  almost all ramp region was detected.

## 5. CONCLUSIONS AND DISCUSSIONS

This work investigates how the GA and the CFAR Coefficient of Variation Detector method detect edge evidence. The two detectors worked similarly when applied to the simulated images tests  $T_1$  and  $T_2$ . However, the Coefficient of Variation Detector finds multiple edges in for these images which does not happen when using GA.

We can point out that the detectors work differently on the  $T_3$  test, while for GA, the evidence of edges was shifted to the center on the ramp. The Coefficient of Variation Detector finds almost the entire ramp region as edges and would need further processing to narrow the edge in that area.

In all test performed the GA showed an advantage over the Coefficient of Variation Detector as it detects only one pixel as edge evidence.

On the other hand, GA compared with Variable Coefficients Detector presents the limitation of defining the region of interest for edge detection and the lines for detecting the transition point between Wishart distributions. At the same

time, the Coefficient of Variation Detector method can be applied to the entire image.

As a future work we plan to apply these methods to real PolSAR images and also investigate the values of  $\mu_1$  and  $\mu_2$  related to the values added to the Wishart distribution.

## 6. REFERENCES

- [1] A. C. Frery, J. Jacobo-Berlles, J. Gambini, and M. Mejail, “Polarimetric SAR image segmentation with B-Splines and a new statistical model,” *Multidimension. Syst. Signal Process.*, vol. 21, pp. 319–342, 2010.
- [2] J. Gambini, M. Mejail, J. Jacobo-Berlles, and A. C. Frery, “Feature extraction in speckled imagery using dynamic B-spline deformable contours under the G0 model,” *Int. J. Remote Sens.*, vol. 27, no. 22, pp. 5037–5059, 2006.
- [3] R. Touzi, A. Lopes, and P. Bousquet, “A statistical and geometrical edge detector for SAR images,” *IEEE Trans. Geosci. Remote Sens.*, vol. 26, no. 6, pp. 764–773, Nov 1988.
- [4] A. C. Frery, H.-J. Muller, C. d. C. F. Yanasse, and S. J. S. Sant’Anna, “A model for extremely heterogeneous clutter,” *IEEE Trans. Geosci. Remote Sens.*, vol. 35, no. 3, pp. 648–659, 1997.
- [5] C. C. Freitas, A. C. Frery, and A. H. Correia, “The polarimetric g distribution for SAR data analysis,” *Environmetrics*, vol. 16, no. 1, pp. 13–31, 2005.
- [6] A. A. de Borba, M. Marengoni, and A. C. Frery, “Fusion of evidences for edge detection in PolSAR images,” in *2019 IEEE Recent Advances in Geoscience and Remote Sensing: Technologies, Standards and Applications (TENGARSS)*, Oct 2019, pp. 80–85.
- [7] A. A. De Borba, M. Marengoni, and A. C. Frery, “Fusion of evidences in intensities channels for edge detection in PolSAR images,” *IEEE Geosci. Remote Sens. Lett.*, in press.
- [8] D. Ebert, *Texturing & Modeling: a Procedural Approach*. San Francisco, CA: Morgan Kaufmann, 2003.
- [9] L. Gomez, L. Alvarez, L. Mazorra, and A. C. Frery, “Fully PolSAR image classification using machine learning techniques and reaction-diffusion systems,” *Neurocomputing*, vol. 255, pp. 52–60, 2017.
- [10] J. Schou, H. Skriver, A. Nielsen, and K. Conradsen, “Cfar edge detector for polarimetric sar images,” *IEEE Transactions on Geoscience and Remote Sensing*, vol. 41, no. 1, pp. 20–32, 2003.